Available online at www.sciencedirect.com
SCIENCE DIRECT®
Journal of Organometallic Chemistry 682 (2003) 163–171
Journal of Organometallic Chemistry
www.elsevier.com/locate/jorganchem

Effects of metal atom motion and ring rotation in iron organometallics. Synthesis of isotopically labelled nonamethyl [^{57}Fe]ferrocene

Rolfe H. Herber [a,*], Israel Nowik [a], Herwig Schottenberger [b], Klaus Wurst [b], Norbert Schuler [b], Adrian Gallus Mueller [b]

[a] *Racah Institute of Physics, The Hebrew University of Jerusalem, 91904 Jerusalem, Israel*
[b] *Institut für Allgemeine, Anorganische und Theoretische Chemie, Leopold Franzens Universität, Innrain 52a, A-6020 Innsbruck, Austria*

Received 8 April 2003; received in revised form 17 June 2003; accepted 17 June 2003

Abstract

Temperature dependent ^{57}Fe Mössbauer effect studies on nonamethyl ferrocene (NMF), have been carried out on isotopically enriched material over the temperature range $90 < T < 290$ K. These measurements have led to the elucidation of the dynamical behaviour of the iron atom and reflect the onset of ring rotation and libration. These results are compared to corresponding data for ferrocene and related compounds. A convenient small scale synthesis suited for the preparation of ^{57}Fe-enriched nonamethylferrocene which allows its easy separation in pure form, is also presented. With the exception of nonamethylferrocene, which is unresolvable due to its lattice-neighbour related conformational ring disorders, X-ray structure determinations of all new compounds of the reaction sequence, and of the starting compound hydroxymethyloctamethylferrocene (octamethylferrocenyl methanol) have been performed.

Keywords: Octamethylferrocene derivatives; ^{57}Iron labelled; X-ray structures; Mössbauer spectroscopy

1. Introduction

Temperature-dependent ^{57}Fe Mössbauer effect spectroscopy has proven itself to be a powerful technique in the elucidation of the details of the metal atom motion in iron organometallics. In particular, recent studies from these laboratories [1–3] have shown that the details of this motion can be related to the molecular level architecture of ferrocene-related solids, and can lead to a better understanding of the macroscopic properties of these compounds which have found considerable use in opto-electronics and chemical sensor applications. An unexpected observation relative to the metal atom motion in ferrocene-related solids was the demonstration [4,5] that in a number of such solids derived from octamethyl ferrocene [η^5-(Cp(Me)$_4$]$_2$Fe (OMF), the recoil-free fraction (f) observed in a Mössbauer spectrum effectively became unobservable at temperatures well below the melting point. Since the area under the resonance curve in a Mössbauer spectrum is proportional to the recoil-free fraction, and the latter is directly related to the mean-square-amplitude of vibration (msav, $\langle x^2 \rangle$) of the metal atom by the relationship

$$f = \exp(-k^2 \langle x^2 \rangle)$$

where k is the wave number of the Mössbauer γ-ray, it follows that the large reduction in the resonance effect must be due to a large increase of $\langle x^2 \rangle$ with increasing temperature. In the case of octamethylferrocene compounds where one proton of a Cp ring may be substituted by an additional small group such as $-C\equiv CH$ or $-CH=CH_2$, the onset of ring rotation results in both an increase of the ring-ring distance as well as a librational motion of one of the rings with respect to the

* Corresponding authors. Tel.: +972-2-6584-347; fax: +972-2-6586-347; Tel: +43-512-507-5120.
E-mail addresses: herber@vms.huji.ac.il (R.H. Herber), herwig.schottenberger@uibk.ac.at (H. Schottenberger).

0022-328X/03/$ - see front matter © 2003 Elsevier B.V. All rights reserved.
doi:10.1016/S0022-328X(03)00778-2

other. This "gear-wheel" effect leads to a marked increase of $\langle x^2 \rangle$, and hence to a pronounced decrease in the resonance effect with increasing temperature. In the case of octamethylferrocene ($T_{MP} = 431$ K), the "vibrational anomaly" occurs at ~ 349 K, that is at a reduced temperature $T_R = T/T_{MP}$ of 0.81 [4]. In the case of ethynyl(octamethyl)ferrocene [6] ($T_{MP} = 246$ K), this anomaly occurs at $T_R \sim 0.56$ [5], while in ethenyl(octamethyl)ferrocene ($T_{MP} = 432$ K), this anomaly occurs at $T_R \sim 0.53$ [7]. Furthermore, it is interesting to note that in a recent quasi-elastic nuclear forward-scattering experiment on ethynyl(octamethyl)ferrocene reported by Asthalter et al. [8] a very similar dynamical behaviour of the iron atom was reported. In that study, a "hysteresis" of about 25 K in the metal atom motion was documented in detail. This hysteresis, which is also observed in the ^{57}Fe Mössbauer experiments—albeit somewhat smaller—appears to be characteristic of the phase transition involving the onset on warming (and cessation on cooling) of ring rotation in this solid.

A previous study [9] of the metal atom motion in nonamethylferrocene (NMF), [η^5-Cp(CH$_3$)$_5$]Fe[η^5-(Cp(CH$_3$)$_4$], showed that a similar effect to that noted in OMF was also present here, although its onset was at a significantly lower temperature. A detailed study of NMF in the temperature range near the anomaly was hampered by the very small resonance effect observed, which in turn requires long data acquisition times. In order to overcome this limitation, a sample of NMF enriched in ^{57}Fe (to 95%, while the natural abundance is 2.21%) was prepared as discussed below, and subjected to a detailed temperature-dependent Mössbauer study in both warming and cooling regimes. The results of this study are detailed herein.

2. Results and discussion

As is true of all previously examined diamagnetic ferrocenyl compounds, the Mössbauer spectra over the temperature range used in the present study ($90 \leq T \leq 273$ K) consist of well resolved doublets corresponding to a single iron site in the structure. The line widths in a temperature region where saturation effects can be ignored (vide infra) are approximately 0.23 mm s^{-1}. A summary of the hyperfine parameters and related quantities is given in Table 1. The temperature dependence of the isomer shifts (IS) is summarized in Fig. 1. In the high temperature limit, that is above ~ 200 K, this parameter is well fitted by a linear regression with a slope of $-(4.160.07) \times 10^{-4}$ mm s^{-1} K^{-1} (correlation coefficient 0.98 for 25 data points) leading to an effective vibrating mass $M_{eff} = 1001.6$ daltons [10], indicative of strong covalency in the Fe-η^5 Cp bonding. As is seen from the figure, there is no significant discontinuity in dIS/dT over the entire temperature range.

Table 1
Summary of Mössbauer data for nonamethyl[^{57}Fe]ferrocene (**4**)

Parameter	Value	T Range	Multiplier	Units
IS (90 K)	0.5070.006			mm s^{-1}
QS (90 K)	2.4640.006			mm s^{-1}
$-$dIS/dT	4.1610.065	200–290	10^{-4}	mm s^{-1} K^{-1}
M_{eff}	1001.6	200–290		daltons
Area ratio (R)	1.000.01	90–290		

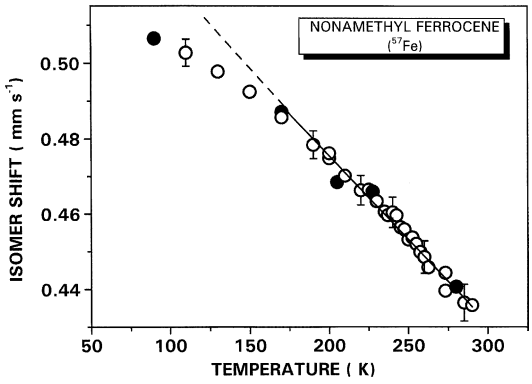

Fig. 1. Temperature dependence of the IS parameter for NMF. The slope of the high temperature region of this data set (solid line) is $-(4.160.06) \times 10^{-4}$ mm s^{-1} K^{-1} from which $M_{eff} \sim 100$ daltons. The open circles represent data acquired in a warming mode between data points, while the full circles refer to cooling data, showing the reversibility of the data with temperature.

The temperature dependence of the quadrupole splitting (QS) is shown in Fig. 2. In contrast, there is a significant change in slope (dQS/dT) at ~ 210 K. The low temperature data show that QS is not a sensitive function of temperature as has been previously noted in the literature [11]. The small negative temperature dependence in this region can be readily accounted for by thermal expansion of the covalent lattice, as has been noted previously. Above the transition point, this temperature dependence becomes significantly more negative. In this context it is appropriate to note that spectra were acquired both in a warming and cooling

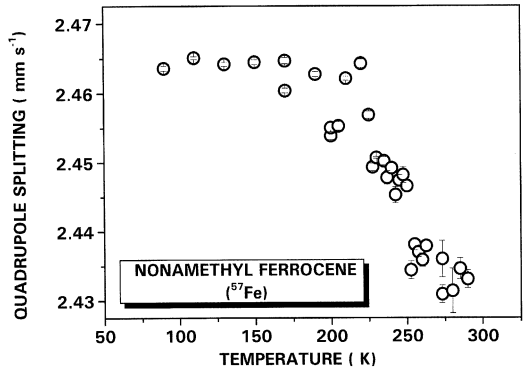

Fig. 2. Temperature dependence of the QS parameter for NMF.

mode, and there is no evidence for non-reversibility in these data.

The temperature dependence of the recoil-free fraction, as reflected in the area under the resonance curve, is summarized in Fig. 3 in which the abscissa is expressed in terms of T_R, the ratio of the experimental temperature to the melting point of NMF, 4812 K. Expressing the abscissa in terms of T_R not only emphasizes the early onset of the recoil-free fraction anomaly in NMF, but also permits a ready comparison with the corresponding $f(T)$ data for the parent ferrocene. Before considering in detail the significance of these data, a number of supportive comments appear to be appropriate. First, the data obtained with a natural abundance ^{57}Fe sample of NMF (star data points) and those obtained with the ^{57}Fe-enriched sample (full circles) are in good agreement with each other as expected. In this context, however, it should be noted that because of the large resonance effects observed for the latter (especially at low temperatures) the data were fitted using a transmission integral program [12] to correct the area under the resonance curve for saturation effects in the spectra. The use of such a transmission integral fitting procedure has been discussed earlier [3,13]. Second, the temperature dependence of $\ln f$ is characterized by a much more gradual decrease with increasing temperature than was noted for OMF, OMF–C≡CH, and OMF–CH=CH_2. Nonetheless, the decrease in $\ln f$ is very pronounced at $T_R > \sim 0.45$, although this is some 250 degrees below T_{MP}! Finally, the corresponding data for ferrocene are included in Fig. 3 from which it can be seen that the resonance effect here is still readily observable at T_R values well above 0.75. In this compound, it is clear that the "gear wheel effect" attributed to the nonamethyl compounds, which confers both librational as well as rotational motion to the rings relative to each other, is absent. A behaviour quite similar to that observed for ferrocene is also operational in decamethyl ferrocene [η^5-Cp$(CH_3)_5]_2$Fe where, at sufficiently high temperatures, only rotational motion of the two rings is presumed to be present [9].

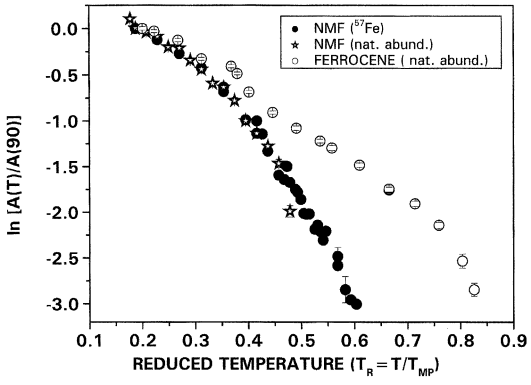

Fig. 3. Temperature dependence of the logarithm of the area under the resonance curve, normalized to the 90 K data point, plotted as a function of the reduced temperature $T_R = T/T_{MP}$. The comparison with the ferrocene data in the high temperature regime illustrates the effect on $\langle x^2 \rangle$ due to the onset of ring rotation and libration in NMF.

A plausible interpretation of these results is as follows: on warming a sample of NMF from 90 to $\sim$ 200 K, the normal thermal expansion factors of a covalent solid readily account for the observed data and are, in fact, in reasonably close agreement with the results obtained for the parent ferrocene [3]. Above $\sim$ 200 K, there is a gradual onset of ring rotation. This ring rotation, which involves an expansion of the ring-ring distance due to mutual steric repulsion of the methyl groups, causes an increase of the ring–metal distance, and hence in an increase of $\langle x^2 \rangle$ of the iron atom, leading to a significant decrease in f as observed.

It is now appropriate to consider why the vibrational anomaly in NMF is less abrupt than it is in the octamethyl ferrocenyl complexes referred to above. It is clear that there is a competition between the effects of the onset of ring rotation which lead to an increase of $\langle x^2 \rangle$ with increasing temperature, and the van der Waals interactions between adjacent molecules of the covalent matrix which tend to offset the former effect on warming. The Fe-ring carbon distance in ferrocene has been reported in numerous X-ray crystallographic studies and is 2.030 Å at 173 K [14], and 2.033 Å at 298 K [15]. In the gas phase, electron diffraction measurements lead to a bond distance of 2.064 Å [16]. The effect of methyl group interactions between the two rings is reflected in the fact that in solid decamethyl ferrocene, in which the methyl groups are bent 3° out of the Cp plane away from the iron atom, the Fe–ring carbon distance determined by X-ray diffraction is 2.049 Å [17], while in the gas phase this value is 2.064 Å [18], identical to that in ferrocene under the same conditions. It is appropriate to note that a similar behaviour to that reported here for NMF has been noted [19] in octamethylferrocenylmethanol [η^5-(Cp$(CH_3)_4$]Fe[(η^5-Cp$(CH_3)_4CH_2OH$], (OMF–CH_2OH), ($T_{MP} = 484$ K), for which T_R for the onset of the $\langle x^2 \rangle$ increase is $\sim$ 0.45, comparable to the value of $T_R \sim 0.47$ for NMF. In comparison, the T_R onset values for OMF, OMF–C≡CH, and OMF–CH=CH_2 are 0.81, 0.56, and 0.53, respectively. Thus, at the lower T_R value, the intermolecular interactions, specifically hydrogen bonding, play a more significant role in the temperature dependence of $\langle x^2 \rangle$ than at higher values of this parameter. As noted earlier [9], the onset of ring rotation and libration in NMF well below r.t. has precluded a detailed single crystal X-ray determination of the structure of this compound at $\sim$300 K. A low temperature (< 220 K) X-ray structure determination would seem to be informative relative to the points raised in this discussion.

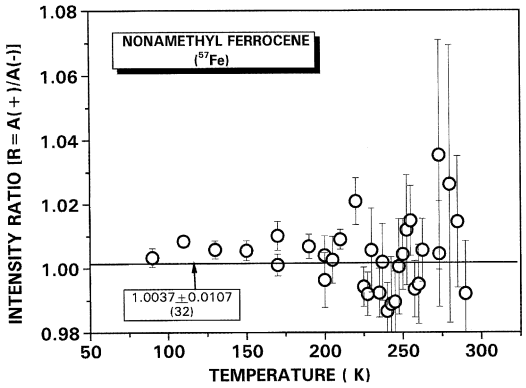

Fig. 4. Temperature dependence of the area ratio of the two components of the quadrupole split doublet in NMF. The absence of a significant departure from unity up to 273 K reflects the isotropy of the metal atom motion in NMF.

A final parameter which should be considered in this discussion is that of the Gol'danskii–Karyagin effect [20] in these solids. This effect, which arises from the anisotropy of the Mössbauer active atom motion with respect to the two major symmetry axes running through the metal atom, is reflected experimentally in the intensity ratio of the two components of the quadrupole doublet; that is, $R = A(+)/A(-)$, where the two areas are those at more positive $(+)$ and more negative $(-)$ velocities with respect to the spectrum centroid. In a number of cyclopentadienyl iron complexes this motional anisotropy has been shown to be a major effect arising from the details of the local molecular architecture, especially when there is a strong anisotropy in the metal atom-ligand bonding present in the structure. The temperature dependence of R for NMF is summarized graphically in Fig. 4 from which it can be seen that R is completely insensitive to temperature over the interval of the Mössbauer measurements ($90 < T < 273$ K). This observation is completely consistent with the damping effects on $\langle x^2 \rangle$ due to the van der Waals interactions at temperatures well below T_{MP}, as referred to above.

3. Synthetic considerations

Nonamethylferrocene **[41311-84-6]** was first mentioned by Nesmeyanov and coworkers [21], and actually was identified by mass spectroscopy as an inseparable by-product obtained from exhaustive Friedel Crafts alkylation: treating ferrocene in heptane with $LiAlH_4$ and $AlCl_3$ in equimolar proportions followed by passage of CH_3Cl gave decamethylferrocene and nonamethylferrocene in about 20% and 50% yields, respectively.

In a later synthetic approach, nonamethylferrocene was obtained from ferrous chloride in tetrahydrofuran by ligand combination of a mixture of pentamethyl- and tetramethylcyclopentadienide. In order to subsequently separate the resulting methylated ferrocenes, preparative HPLC-methods were developed for neutral and oxidized cationic mixtures as well [22]. However, besides the additional problems of chromatographic recovery, if only nonamethylferrocene is desired, two thirds of the enriched iron isotope would be consumed by the unwanted octa- and decamethylferrocene also formed in this statistical approach.

Transition metal catalysed hydrogenations of octamethylferrocene carbaldehyde, **[128925-12-2]**, have not been reported so far. Since handling small quantities of expensive progenitors in an autoclave is likely to involve tedious workup, no attempts have been undertaken to investigate such conversions of this most versatile starting compound in substitution chemistry of octamethylferrocene [23]. Furthermore, the high steric shielding of the aldehyde moiety by adjacent methyl groups may require fine tuned reaction conditions for a clean and complete conversion to NMF.

Therefore, it seemed encouraging to try a small scale preparation by hydride addition to octamethylferrocenylmethylium tetrafluoroborate **[128925-11-1]**, which was reported to be fairly stable for limited periods at low temperatures as an isolated salt [23].

However, the dissolution of this salt in any appropriate solvent to establish homogeneous reaction conditions, which turned out to be necessary for the attack of hydride transfer reagents, is accompanied by the known dimerisation forming 1,2-bis(octamethylferrocenyl) ethane species [23], thus resulting in lower yields and, unfortunately, causing problems of separation. For example, according to nuclear magnetic resonance measurements, a composition of 85% NMF besides 15% 1,2-bis[(octamethyl)ferrocenyl]ethane was found in the apolar fractions when reacting octamethylferrocenylmethylium tetrafluoroborate with lithium triethylborohydride in THF. The ethanediyl-bridged biferrocenium salt, generated in the dimerisation step, obviously undergoes reduction to the neutral apolar species, which prevents its separation by means of standard column chromatography on a preparative scale. Upon addition of lithium or potassium hydride in THF, no NMF could be obtained.

In Wittig reactions involving octamethylferrocenylmethyl triphenylphosphonium bromide **[185543-98-0]**, we regularly observed concomitant degradation of the respective ylide intermediate, affording some trace amounts of NMF after aqueous workup [24]. NMF obtained by this side reaction was the primary source for earlier Mössbauer investigations [9,11a]. The utilization of this reaction sequence for the intended formation of [^{57}Fe]NMF (**4**) also led us to identify a second elimination product, where the bond cleavage of the phosphonium ylide occurs between the phosphorus and a phenylic carbon to form the novel ferrocene substituted

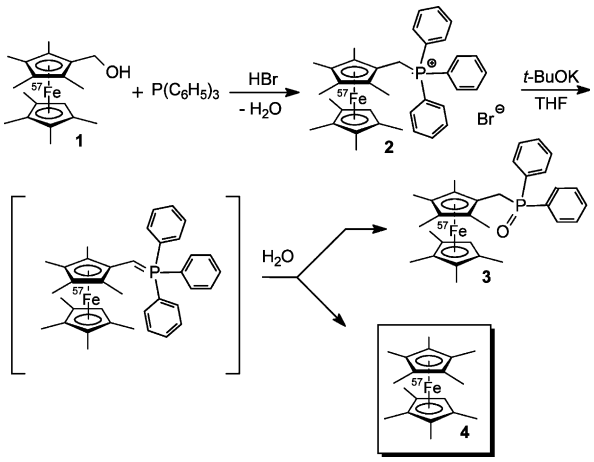

Scheme 1. Small scale synthesis of nonamethylferrocene via phosphonium ylide.

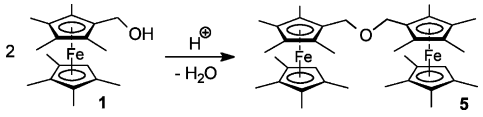

Scheme 2. Protic formation of ether-type dimers from hydroxymethylferrocenes.

phosphine oxide **3**. This derivative will be the subject of future Mössbauer studies [25] (Scheme 1).

The higher polarity of **3** compared to the extremely apolar **4** allows a convenient separation of the product mixture by simple chromatography on basic alumina (see Section 4).

It is worth noting that under acidic conditions, especially in the absence of nucleophilic coreactants, also the conversion of hydroxymethyl-octamethylferrocene, **[128925-13-3]**, to a further by-product, not described previously in the literature, namely di[(octamethylferrocenyl)methyl] ether (**5**) takes place; it is the expected predominant product under conditions of water removal by acidic catalysis. This compound represents the first ether-type product based on octamethylferrocene, its detailed characterisation including Mössbauer studies will also be published in a forthcoming paper (Scheme 2).

3.1. Refinement details of **5** (Fig. 5)

Reflected by the highly distorted thermal ellipsoids of the two tetramethyl–Cp rings, the ring at Fe1 shows a disordering, which could be caused by a free rotation of the ring or by a normal 1:1 disorder in two positions (rotation by 180°). The disorder was not solved and the carbon atoms of the four methyl groups were refined into five positions with an occupation factor of 0.8.

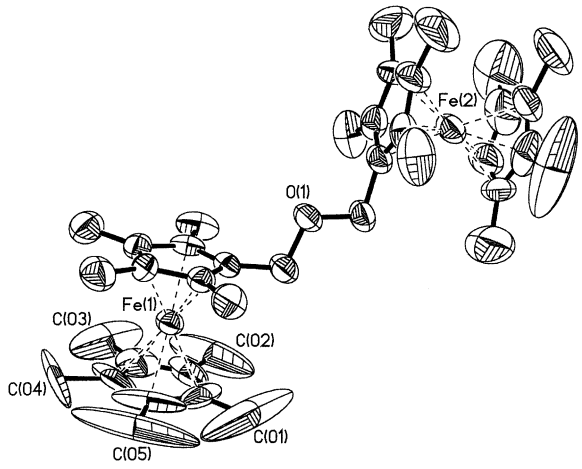

Fig. 5. ORTEP plot of **5** showing 50% of thermal ellipsoids; methyl- and Cp-protons are omitted for clarity.

4. Experimental

4.1. Instrumentation

Bruker AC 300 (NMR), Nicolet 510 FTIR (IR); Varian CH-7 (MS); Nonius Kappa CCD (X-ray). Melting points were determined on a Kofler hot-plate apparatus equipped with a thermocouple (Leica Galen III; Fluke 50S; correction obsolete).

4.2. Synthetic procedures

The starting material for all ferrocenes described in this work, iron(II) chloride enriched in ^{57}Fe, was prepared from >95% enriched metallic iron powder by a modified literature procedure [26]. ^{57}Fe-enriched iron powder (>95%) was purchased from AMT, Advanced Materials Technologies, 7 Mevo Dalya Str., Yehud 56478, Israel; sales@isotope-amt.com.

All organometallic reactions were carried out under inert atmosphere conditions using standard Schlenk techniques. Solvents were distilled, dried and deoxygenated prior to use. Starting compounds not referenced are commercially available. Purchased chemicals were used without any further purification.

^{57}Fe enriched octamethylferrocenyl methanol, **[4115698-09-8]** [19,27], was prepared in analogy to published procedures [23,24] for naturally abundant isotope material, **[128925-13-3]**, starting from the corresponding carbaldehyde [25]. Small scale optimised preparations were applied in analogy to published procedures also for the preparation of ^{57}Fe-enriched octamethylferrocene [28]. All preparations requiring ^{57}Fe-enriched chemicals have been previously checked with unlabelled ferrous chloride and ferrocene starting compounds (vide infra).

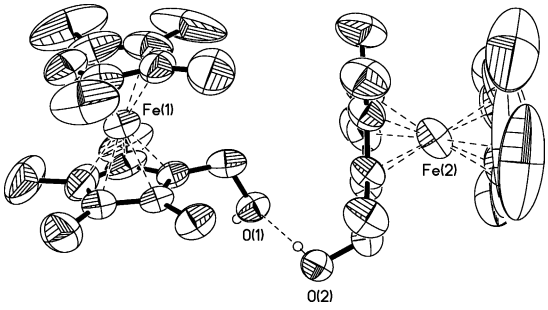

Fig. 6. ORTEP plot of **1** showing 50% of thermal ellipsoids; methyl- and Cp-protons are omitted for clarity.

4.2.1. 1-(Hydroxymethyl)-1′,2,2′,3,3′,4,4′,5-octamethyl[^{57}Fe]ferrocene [415698-09-8] (**[^{57}Fe]1**)

1′,2,2′,3,3′,4,4′,5-Octamethyl[^{57}Fe]ferrocenylcarbaldehyde [25] (120 mg, 0.37 mmol) was dissolved in anhydrous THF (15 ml) under argon to form a red solution, and subsequently cooled to −40 °C. Lithium triethylborohydride (0.55 ml, 0.55 mmol = 1.5 equivalent) was then added dropwise via syringe. The resulting yellow solution was warmed to room temperature (r.t.) and stirred for another 1.5 h. Water (30 ml) was added and most of the THF was removed azeotropically by means of a vacuum line. The resulting suspension was extracted with ether (40 ml) and the organic phase was washed back with water (30 ml) and brine (20 ml). Afterwards, the solvent was reduced in volume to about 2 ml. Subsequent column chromatography on basic alumina (Brockmann III, 9 × 3 cm) in ether yielded **[^{57}Fe]1** (105 mg, 86.7%) as a yellow solid, which was used without further purification in the following step (Fig. 6).

4.2.2. (1′,2,2′,3,3′,4,4′,5-Octamethyl[^{57}Fe]ferrocenyl)methyl-triphenylphosphonium bromide (**[^{57}Fe]2**)

To a solution of **1** (105 mg, 0.32 mmol) in neat toluene (30 ml), triphenylphosphine hydrobromide (109 mg, 0.32 mmol = 1.0 equivalent) was added and the mixture was refluxed in order to azeotropically remove water by means of a Dean–Stark trap for 15 min; during this operation, a yellow solid gradually precipitated. After cooling, the precipitate was filtered through a sintered glass frit (G4). The product was washed twice with ether (10 ml each) and dried to yield analytically pure **[^{57}Fe]2** (174 mg, 73% overall yield). m.p.:192–193 °C; IR (KBr, cm^{-1}): 3052 w, 2960 m, 2939 m, 2898 s, 2854 m, 1585 w, 1481 m, 1436 vs, 1380 m, 1106 s, 1031 m, 997 m, 754 m, 740 s, 692 s, 509 m, 497 s, 472 m, 449 m; ^{1}H-NMR (300.13 MHz, CD_2Cl_2) δ 7.85 (t, 3H, J = 7.3 Hz, Ar), 7.66 (t, 6H, J = 7.3 Hz, Ar), 7.57–7.50 (m, 6H, Ar), 3.98 (s (br), 2H, CH_2), 3.67 (s (br), 1H, H of fec), 1.45 (s, 12H, 4 × CH_3), 1.37 (s, 6H, 2 × CH_3), 0.81 (s, 6H, 2 × CH_3); ^{13}C-NMR (75.47 MHz, CD_2Cl_2) δ 135.51 (Ar-C_{para}), 134.74 (d, J = 9 Hz, Ar-C_{ortho}), 130.26 (d, J = 12 Hz, Ar-C_{meta}), 117.50 (d, J = 84 Hz, Ar-C_{ipso}), 83.55 (d, J = 5 Hz, fec-C), 82.50 (d, J = 5 Hz, fec-C), 82.27 (fec-C), 80.72 (d, J = 2 Hz, fec-C), 72.62 (fec-C), 71.25 (fec-CH), 25.94 (d, J = 43 Hz, CH_2), 11.12, 9.92, 9.29, 9.13 (CH_3); ^{31}P-NMR (121.49 MHz, CD_2Cl_2) δ 12.93 (s, $P(Ph)_3$); M^S (FAB pos.): $[M+H]^+$ calculated: 574.2, found: 574.0.

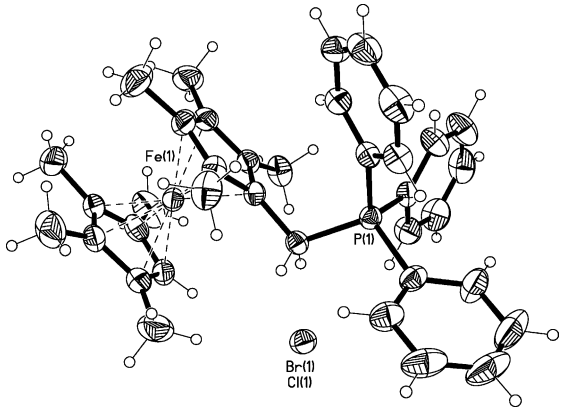

Fig. 7. ORTEP plot of **2** showing 50% of thermal ellipsoids.

4.2.3. X-ray analysis

Single crystals were grown from CD_2Cl_2 (NMR solution). The phosphonium species crystallized with a dichloromethane solvate as a mixed halogenide salt, statistically disordered with respect to the bromide and chloride counterions, in a ratio of 2:1 (formed by partial nucleophilic substitution of the solvent by bromide anion, see Fig. 7).

4.2.4. Refinement details of **[^{57}Fe]2**

2:1 disorder of the chlorine atoms Cl2:ClA and Cl3:Cl3A of the solvent dichloromethane (for hydrogen calculation the carbon atom was split into two parts with equal coordinates and displacement parameters C30–C30A). Another 2:1 disorder (see above) appears for the halide counterions; the same position is occupied by 2/3 bromide Br1 and 1/3 chloride Cl.

4.2.5. (1′,2,2′,3,3′,4,4′,5-Octamethyl[^{57}Fe]ferrocenyl)methyl-diphenylphosphine oxide (**[^{57}Fe]3**) and 1,1′,2,2′,3,3′,4,4′,5-Nonamethyl[^{57}Fe]ferrocene (**[^{57}Fe]4**)

To a precooled (−65 °C), well stirred yellow suspension of (1′,2,2′,3,3′,4,4′,5-octamethyl[^{57}Fe]ferrocenyl)methyl-triphenylphosphonium bromide (**[^{57}Fe]2**) (75 mg, 0.11 mmol) in anhydrous THF (20 ml), ^{t}BuOK (42 mg, 0.37 mmol = 3.4 equivalents) was added all at once under Ar. Afterwards, the cooling bath was removed and the resulting deep red mixture was allowed to reach r.t. over 1.5 h. After warming up to 50 °C for 1.5 h, the now yellow misty suspension was quenched with water (30 ml) and most of the THF was removed

azeotropically by means of a vacuum line. The resulting suspension was extracted with ether (40 ml) and the ethereal phase was washed back with water (2×30 ml) and brine (20 ml). The yellow solution was dried over Na_2SO_4 and the ether was removed to dryness. The crude product was suspended in n-hexane and filtered through cotton wool. The insoluble part was dissolved in ether and chromatographed on basic alumina (Brockmann III, 8×3 cm) in ether to yield **[^{57}Fe]3** (19 mg, 32.3%) as a pale yellow solid. The filtrate was chromatographed on basic alumina (Brockmann III, 5×3 cm) in *n*-hexane to yield **[^{57}Fe]4** (15 mg, 41.9%) as a yellow solid.

4.2.6. Data for *[^{57}Fe]3*

M.p.: 146–148 °C; IR (KBr, cm^{-1}): 3052 m, 2962 s, 2940 s, 2900 vs, 2856 m, 1436 s, 1378 m, 1189 vs, 1176 s, 1118 m, 1027 m, 738 s, 721 m, 696 m, 530 m, 501 m, 474 m; ^{1}H-NMR (300.13 MHz, CD_2Cl_2) δ 7.68–7.61 (m, 4H, Ar), 7.54–7.40 (m, 6H, Ar), 3.20 (d, 2H, $J = 11.6$ Hz, CH_2), 3.17 (s, 1H, H of fec), 1.66, 1.65, 1.60, 1.34 (each: s, 6H, $2 \times CH_3$); ^{13}C-NMR (75.47 MHz, CD_2Cl_2) δ 134.40 (d, $J = 95$ Hz, Ar-C_{ipso}), 131.72 (d, $J = 3$ Hz, Ar-C_{para}), 131.45 (d, $J = 9$ Hz, Ar-C_{ortho}), 128.55 (d, $J = 10$ Hz, Ar-C_{meta}), 80.34, 80.01, 79.86, 74.10 (fec-C), 71.22 (fec-CH), 29.87 (d, $J = 68$ Hz, CH_2), 11.18, 10.29, 9.85, 9.25 (CH_3); ^{31}P-NMR (121.49 MHz, CD_2Cl_2) δ 26.37 (s, O=P(Ph)$_2$); HR-EIMS: [$M^{\bullet +}$] calc.: 513.19363, found: 513.1936.

4.2.7. Data for *[^{57}Fe]4*

M.p.: 180–182 °C (partial melting due to a phase transition between 130–135 °C); IR (KBr, cm^{-1}): 2962 m, 2942 m, 2898 m, 2854 m, 1375 m, 1261 s, 1097 vs, 1025 vs, 802 vs, 455 m; ^{1}H-NMR (300.13 MHz, CD_2Cl_2) δ 3.16 (s, 1H, H of fec), 1.70 (s, 15H, $5 \times CH_3$), 1.69 (s, 6H, $2 \times CH_3$), 1.64 (s, 6H, $2 \times CH_3$); ^{13}C-NMR (75.47 MHz, CD_2Cl_2) δ 79.95, 79.63, 78.93 (fec-C), 70.96 (fec-CH), 11.18, 9.88, 9.26 (CH_3); HR-EIMS: [$M^{\bullet +}$] calc.: 312.1467, found: 312.15008.

4.2.8. *(1′,2,2′,3,3′,4,4′,5-Octamethylferrocenyl)methyldiphenylphosphine oxide (**3**), and 1,1′,2,2′,3,3′,4,4′,5-Nonamethylferrocene, **[41311-84-6]** (**4**) (Fig. 8)*

To a cooled (−65 °C) and well stirred yellow suspension of (1′,2,2′,3,3′,4,4′,5-octamethylferrocenyl)methyltriphenylphosphonium bromide (**2**), (215 mg, 0.33 mmol) in dry THF (40 ml), ^{t}BuOK (123 mg, 1.10 mmol = 3.3 equivalents) was added all at once under Ar. The resulting deep red mixture was stirred for 2.5 h at 0 °C in an ice-water bath. Afterwards, water (40 ml) was added. Most of the THF was removed azeotropically in vacuo, the yellow suspension was extracted with ether (60 ml) and the ethereal phase was washed back with water (2×30 ml) and brine (30 ml). The yellow solution was dried over Na_2SO_4 and the ether was removed to dryness. The crude product was suspended in *n*-hexane and filtered through cotton wool. The insoluble part was dissolved in ether and chromatographed on basic alumina (Brockmann III, 8×3 cm) in ether to yield **3** (33 mg, 20%) as a pale yellow solid. The filtrate was chromatographed on basic alumina (Brockmann III, 6×3 cm) in *n*-hexane to yield **4** (40 mg, 39%) as a yellow solid.

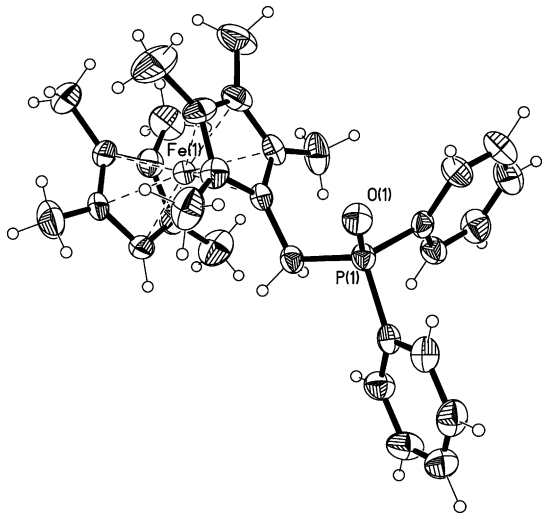

Fig. 8. ORTEP plot of **3** showing 50% of thermal ellipsoids.

Performing the reaction under the same conditions but warming to r.t. over 3 h after addition of ^{t}BuOK yielded **3** in 22.% and **4** in 38%. When heated to 55 °C for 3 h after addition of ^{t}BuOK the yield of **3** increased to 29%, but the yield of **4** decreased slightly to 35%.

4.2.9. Data for *3*

M.p.: 169–171°C; IR (KBr, cm^{-1}): 3052 m, 2962 m, 2942 m, 2898 s, 2856 m, 1436 s, 1380 m, 1371 m, 1186 vs, 1118 m, 1027 m, 740 s, 719 s, 701 m, 526 s, 509 m, 476 m, 410 m; ^{1}H-NMR (300.13 MHz, CD_2Cl_2) δ 7.67–7.60 (m, 4H, Ar), 7.54–7.38 (m, 6H, Ar), 3.22 (d, 2H, $J =$ 11.6 Hz, CH_2), 3.15 (s, 1H, H of fec), 1.67, 1.66, 1.60, 1.35 (each: s, 6H, $2 \times CH_3$); ^{13}C-NMR (75.47 MHz, CD_2Cl_2) δ 133.90 (d, $J = 95$ Hz, Ar-C_{ipso}), 131.71 (d, $J = 2$ Hz, Ar-C_{para}), 131.45 (d, $J = 9$ Hz, Ar-C_{ortho}), 128.55 (d, $J = 10$ Hz, Ar-C_{meta}), 80.28, 80.24, 79.93, 79.78, 74.06 (fec-C), 71.18 (fec-CH), 29.89 (d, $J = 68$ Hz, CH_2), 11.18, 10.29, 9.85, 9.25 (CH_3); ^{31}P-NMR (121.49 MHz, CD_2Cl_2) δ 26.55 (s, O=P(Ph)$_2$); MS(EI pos.): [$M^{\bullet +}$] calc.: 512.2, found: 512.2. X-ray analysis: single crystals were grown from CH_2Cl_2–*n*-hexane = 1:1.

4.2.10. Data for *4*

M.p.: 163 °C; IR (KBr, cm^{-1}): 3054 w, 2962 s, 2940 s, 2896 vs, 2854 s, 1475 m, 1448 m, 1425 m, 1375 s, 1261 m, 1068 m, 1027 s, 819 m, 804 m, 457 s; ^{1}H-NMR (300.13 MHz, CD_2Cl_2) δ 3.18 (s, 1H, H of fec), 1.65 (s, 21H, $7 \times CH_3$), 1.60 (s, 6H, $2 \times CH_3$); ^{13}C-NMR (75.47 MHz,

Table 2
Crystal data and structure refinement for **1**, **2**, **3** and **5**

Octamethylferrocenyl–methyl compound	**1** OMF–CH_2–OH	[^{57}Fe]**2** OMF–CH_2–$P(C_6H_5)_3X^-$	[^{57}Fe]**3** OMF–CH_2–$PO(C_6H_5)_2$	**5** OMF–CH_2–O–CH_2–OMF
Molecular formula	$C_{19}H_{28}FeO$	$C_{37}H_{42}FeP^+Br^-_{0.67}Cl^-_{0.33}\cdot CH_2Cl_2$	$C_{31}H_{37}FeOP$	$C_{38}H_{54}Fe2O$
Formula weight	328.26	723.54	512.43	638.51
Crystal system	Monoclinic	Monoclinic	Monoclinic	Monoclinic
Space group	$C2/c$ (No.15)	$P2_1/n$ (No.14)	$P2_1/c$ (No.14)	$P2_1/n$ (No.14)
a (pm)	3838.0(3)	957.35(2)	1160.01(3)	1796.7(1)
b (pm)	871.15(4)	2201.02(4)	2330.02(7)	857.25(6)
c (pm)	2835.7(2)	1696.54(3)	1123.21(2)	2237.2(1)
α (°)	90	90	90	90
β (°)	132.240(2)	91.306(2)	116.010(2)	90.366(3)
γ (°)	90	90	90	90
V (nm^3)	7.0192(8)	3.57393(12)	2.72838(12)	3.4457(3)
Z	16	4	4	4
Temperature (K)	2933(2)	233(2)	233(2)	233(2)
D_{calc} (Mg m^{-3})	1.243	1.345	1.247	1.231
Absorption coefficient (mm^{-1})	0.857	1.412	0.632	0.869
F(000)	2816	1504	1088	1368
Colour, habit	Yellow prism	Yellow prism	Yellow prism	Yellow prism
Crystal size (mm)	0.4 × 0.2 × 0.1	0.3 × 0.2 × 0.15	0.6 × 0.4 × 0.06	0.25 × 0.18 × 0.14
Data collection θ range (°)	1.94–20.00	1.85–25.00	1.75–24.00	1.45–20.00
Index ranges	$0 \le h \le 40$; $-8 \le k \le 9$; $-29 \le l \le 22$	$0 \le h \le 11$; $-26 \le k \le 26$; $-20 \le l \le 20$	$-13 \le h \le 0$; $-26 \le k \le 26$; $-11 \le l \le 12$	$0 \le h \le 17$; $-8 \le k \le 8$; $-21 \le l \le 21$
Reflections collected	8535	22 308	14 139	11 748
Independent reflections	3162 [$R_{int} = 0.0329$]	6283 [$R_{int} = 0.0307$]	4275 [$R_{int} = 0.0393$]	3216 [$R_{int} = 0.0726$]
Number of reflections with $I > 2\sigma(I)$	2639	5285	3505	2234
Abs correction	None	None	None	None
Refinement method	Full-matrix least-squares on F^2	Full-matrix least-squares on F^2	Full-matrix least-squares on F^2	Full-matrix least-squares on F^2
Data/restraints/parameters	3037/2/399	6283/0/414	4275/0/316	3216/3/391
Goodness-of-fit on F^2	1.058	1.031	1.030	1.038
Final R indices [$I > 2\sigma(I)$]	$R_1 = 0.0672$; $wR_2 = 0.1544$	$R_1 = 0.0306$; $wR_2 = 0.0713$	$R_1 = 0.0383$; $wR_2 = 0.0887$	$R_1 = 0.0634$; $wR_2 = 0.1750$
R indices (all data)	$R_1 = 0.0804$; $wR_2 = 0.1709$	$R_1 = 0.0417$; $wR_2 = 0.0758$	$R_1 = 0.0520$; $wR_2 = 0.0938$	$R_1 = 0.0945$; $wR_2 = 0.1924$
Largest difference peak and hole (e nm^{-3})	553 and −620	243 and −306	551 and −274	469 and −277

CD_2Cl_2) δ 80.00, 79.68, 78.96 (fec-C), 70.99 (fec-CH), 11.18, 9.88, 9.26 (CH_3); MS(EI pos.): $M^{\bullet +}$ calc.: 312.15, found: 312.1.

4.2.11. X-ray measurement and structure determination of *1*, *[^{57}Fe]2*, *[^{57}Fe]3* and *5*

The data collection was performed on a Nonius Kappa CCD equipped with graphite-monochromatised Mo–K_α-radiation ($\lambda = 0.71073$ Å) and a nominal crystal to area detector distance of 36 mm. Intensities were integrated using DENZO and scaled with SCALEPACK [29]. Several scans in ϕ and ω direction were made to increase the number of redundant reflections, which were averaged in the refinement cycles. The structures were solved with direct methods SHELXS86 [30] and refined against F^2 (SHELX97) [31]. Hydrogen atoms at carbon atoms were added geometrically and refined using a riding model, hydrogen atoms at the hydroxyl groups of **1** was refined regular with isotropic displacement parameters. All non-hydrogen atoms were refined with anisotropic displacement parameters.

Crystallographic data are collected in Table 2.

4.3. Mössbauer spectroscopic investigations

The Mössbauer spectrometer, its method of calibration, the method of data reduction and thermal control have been described earlier [1,13,32].

A 5.8 mg sample of solid nonamethylferrocene was ground with quartz powder to reduce crystallite size, mixed with BN to ensure random crystallite orientation with respect to the optical axis of the experiment, and packed into a plastic sample holder which was, in turn, transferred to a variable temperature cryostat as described earlier [13]. The details of the spectroscopic measurements, as well as the data reduction and transmission integral corrections have also been discussed previously. Spectrometer calibration was effected

using an 18.81 mg cm^{-2} natural abundance α-Fe absorber at room temperature, and all isomer shifts are reported with respect to the centroid of this spectrum.

5. Supplementary material

Tables of crystal data and structure refinement details, anisotropic thermal parameters, fractional atomic coordinates and isotropic thermal parameters for the non-hydrogen atoms, all bond lengths and angles, and fractional atomic coordinates for the hydrogen atoms have been deposited with the Cambridge Crystallographic Data Centre, CCDC nos. 212215 (**1**), 212216 (**[^{57}Fe]2**), 212217 (**[^{57}Fe]3**) and 212218 (**5**). Copies of this information may be obtained free of charge from The Director, CCDC, 12 Union Road, Cambridge CB2 1EZ, UK (Fax: +44-1223-336033; e-mail: deposit@ccdc.cam.ac.uk or www: http://www.ccdc.cam.ac.uk).

Acknowledgements

The authors (R.H.H. and I.N.) are indebted to the Israel Ministry of Science and the Racah Institute for financial support. We thank Professor Karl-Hans Ongania for recording the high resolution mass spectra.

References

[1] I. Nowik, R.H. Herber, J. Phys. Chem. Solids 64 (2003) 313.
[2] G. Laus, H. Schottenberger, N. Schuler, K. Wurst, R.H. Herber, J. Chem. Soc. Perkin Trans. 2 (2002) 1445.
[3] R.H. Herber, I. Nowik, Hyperfine Interactions 136/7 (2001) 699.
[4] I. Nowik, R.H. Herber, Inorg. Chim. Acta 310 (2000) 191.
[5] H. Schottenberger, M.R. Buchmeiser, R.H. Herber, J. Organomet. Chem. 612 (2000) 1.
[6] H. Schottenberger, K. Wurst, R.H. Herber, J. Organomet. Chem. 625 (2001) 200.
[7] R.H. Herber, unpublished results. The author is indebted to Dr. Ingrid Kohl and Professor Erwin Mayer for DSC data pertaining to OMF–CH=CH_2
[8] T. Asthalter, H. Franz, U. van Bürck, K. Messel, E. Schreier, R. Dinnebier, J. Phys. Chem. Solids 64 (2003) 677.
[9] R.H. Herber, in: M. Gielen, R. Willem, B. Wrackmeyer (Eds.), Unusual Structures and Physical Properties in Organometallic Chemistry, Wiley, West Sussex, UK, 2002, pp. 207–218.
[10] R.H. Herber, in: R.H. Herber (Ed.), Chemical Mössbauer Spectroscopy, Plenum Press, New York, 1984, pp. 199–216.
[11] (a) R.H. Herber, Inorg. Chim. Acta 291 (1999) 74;
(b) A. Houlton, J.R. Miller, R.M.G. Roberts, J. Silver, J. Chem. Soc. Dalton Trans. (1991) 467 (and references cited therein).
[12] G.K. Shenoy, J.M. Friedt, H.J. Maletta, S.L. Ruby, in: I.J. Gruverman, C.W. Seidel, D.K. Dieterly (Eds.), Mössbauer Effect Methodology, vol. 9, Plenum Press, New York, 1974, pp. 277–305.
[13] R.H. Herber, I. Nowik, Solid State Sci. 4 (2000) 691.
[14] C.P. Brock, Y. Fu, Acta Crystallogr. B53 (1997) 928.
[15] P. Seiler, J.D. Dunitz, Acta Crystallogr. B35 (1979) 1068; see also P. Seiler, J.D. Dunitz, Acta Crystallogr. B35 (1979) 2020.
[16] L. Phillips, A.R. Lacey, M.K. Cooper, J. Chem. Soc. Dalton (1988) 1383.
[17] D.P. Freyberg, J.L. Robbins, K.N. Raymond, J.C. Smart, J. Am. Chem. Soc. 101 (1979) 892.
[18] A. Almenningen, A. Haaland, S. Samdal, J. Brunvoll, J.C. Smart, J. Organomet. Chem. 173 (1979) 293.
[19] R.H. Herber, I. Nowik, T. Asthalter, E. Reichel, H. Schottenberger, J. Organomet. Chem. 642 (2002) 203.
[20] See Ref. [1] and references therein.
[21] A.N. Nesmeyanov, N.S. Kochetkova, A.M. Vainberg, Yu.K. Krynkina, Doklady Akademii Nauk SSSR 207 (1972) 868.
[22] (a) J. Maynollo, diploma thesis, Innsbruck, 1991;
(b) M. Andre, P. Jaitner, J. Maynollo, H. Schottenberger, XVth International Conference on Organometallic Chemistry, Warsaw, August 9–14, 1992, book of abstracts, P153.
[23] C.H. Zou, M.S. Wrighton, J. Am. Chem. Soc. 112 (1990) 7578.
[24] A. Hradsky, B. Bildstein, N. Schuler, H. Schottenberger, P. Jaitner, K.-H. Ongania, K. Wurst, J.-P. Launay, Organometallics 16 (1997) 392.
[25] A.G. Mueller. E. Reichel, H. Kopacka, H. Schottenberger, K. Wurst, K.H. Ongania, R.H. Herber, submitted to *J. Organomet. Chem.*
[26] M. Aresta, C.F. Nobile, D. Petruzelli, Inorg. Chem. 16 (1977) 1817.
[27] R.H. Herber, I. Nowik, Hyperfine Interactions 141/2 (2002) 297.
[28] G. Schmitt, S. Özman, Chem. Ztg. 100 (1976) 143.
[29] Z. Otwinowski, W. Minor, Methods Enzymol. 276 (1997) 307.
[30] (a) G.M. Sheldrick, SHELXS-86: Program for Crystal Structure Solutions, University of Göttingen, Göttingen, Germany, 1986;
(b) G.M. Sheldrick, SHELXL-93: Program for the Refinement of Crystal Structures, University of Göttingen, Göttingen, Germany, 1993.
[31] Sheldrick, G.M.: Program package SHELXTL V.5.1, Bruker Analytical X-Ray Instruments Inc, Madison, USA, 1997
[32] (a) R.H. Herber, E. Bauminger, I. Felner, J. Chem. Phys. 104 (1996) 1;
(b) R.H. Herber, Hyperfine Interactions 108 (1997) 549 (and references cited therein).